Intraplate Stress of the Pacific Plate Inferred from Global Mantle Flow Models

Project Representative
Masaki Yoshida　Volcanoes and Earth's Interior Research Center, Research Institute for Marine Geodynamics, Japan Agency for Marine- Earth Science and Technology

Authors
Masaki Yoshida*[1]

*[1] Volcanoes and Earth's Interior Research Center, Research Institute for Marine Geodynamics, Japan Agency for Marine-Earth Science and Technology

Keywords：intraplate stress, driving force, Pacific plate, instantaneous mantle flow, numerical model

1. Introduction

The intraplate stresses of the Earth's oceanic plates, which can be measured by geophysical and geological approaches (i.e., focal mechanisms, borehole breakouts, in situ stress measurements, fault slip analysis, volcanic vent alignments, etc.) is crucial for understanding the origin of the intraplate stress field of plate motion. The Pacific plate, which is the largest oceanic plate on Earth, has implications for achieving a general understanding of the intraplate stress. However, because there are a few large seismicities and thus few observational datasets for the stable part of the Pacific plate far from the spreading ridges and trenches [e.g., 1], it remains difficult to infer the intraplate stress field from observation data alone.

Here, based on a recent publication [2], I report the numerical studies on the stress state of the entire Pacific plate using an instantaneous global mantle flow calculation technique.

2. Methods

A mantle flow model confined in a three-dimensional (3D) spherical shell domain along spherical polar coordinates (r, θ, φ) was used to obtain the intraplate stress field in the global domain. The mantle was modeled as a viscous fluid with an infinite Prandtl number, and the instantaneous mantle flow was numerically calculated using the mantle convection code "ConvGS" based on the finite-volume method and the Yin-Yang grid. The mechanical conditions for the top and bottom surface boundaries of the mantle were impermeable and shear stress-free.

The density anomaly ($\Delta\rho$) and temperature anomaly (ΔT) in the mantle were converted from the S-wave velocity anomaly (δV_S) structure from the "TX2019slab" seismic tomography model [3] as follows:

$$\Delta\rho(r, \theta, \varphi) = \rho_{ref}(r) \cdot B_S(r) \cdot \delta V_S(\theta, \varphi) \quad (1)$$

$$\Delta T(r, \theta, \varphi) = -A_S^{-1}(r) \cdot \delta V_S(\theta, \varphi) \quad (2)$$

where $\rho_{ref}(r)$ is the reference density with a function of radius, $A_S(r)$ is the temperature derivative of the S-wave seismic velocity anomaly, $\alpha(r)$ is the coefficient of thermal expansion, and $B_S(r) = \alpha(r)/A_S(r)$ is the conversion factor. The density anomaly in the regions with high-seismic-velocity anomalies above a depth of 300 km was set to zero to remove compositional effects in the shallower part of the upper mantle. Instead, the configuration of subducting slabs was constructed from a global slab configuration model, "Slab2" [4]. Figure 1 shows an example of the density anomaly and viscosity structures used in this study. For the details of the numerical model, refer to [2].

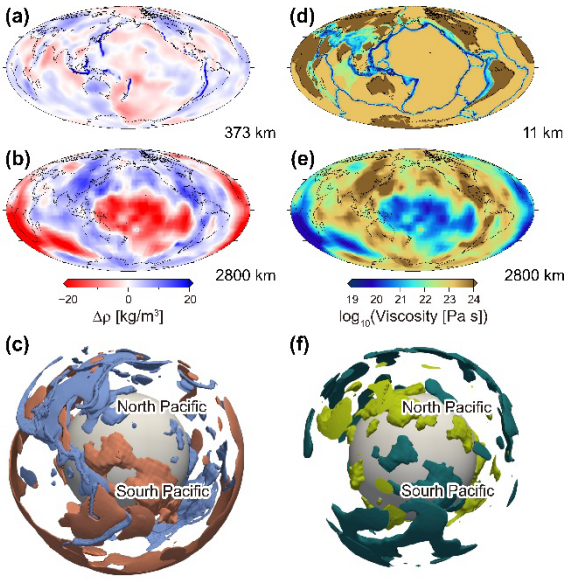

Fig. 1. Numerical model used in the present study. (a, b, d, and e) The density anomaly ($\Delta\rho$) structure at depths of (a) 373 km and (b) 2,800 km, and the viscosity structure (d) near the top surface and (e) at a depth of 2,800 km. (c and f) The 3D isosurfaces of (c) density anomaly and (f) viscosity structures in the whole mantle (the bottom depth is 2,891 km). Modified from Fig. 3 of [2].

3. Results

I studied a lot of numerical models under different free parameters and geophysical conditions [2]. Here, I report a numerical result for the reference model (termed "Model Ref") with a viscosity contrast between the lithosphere and the upper mantle of 300 and a viscosity contrast between the lower and upper mantle of 30.

Figure 2 shows the distribution of the viscosity and horizontal velocity fields near the entire top surface boundary (Fig. 2a), the distribution of the "stress ratio (R_S)" [e.g., 5] in each faulting

regime near the entire top surface boundary (Fig. 2b), and the distribution of the horizontal principal deviatoric stress axes in the Pacific plate (Fig. 2c). It was found that the direction and speed of the Pacific plate are comparable to the observed plate motions (Fig. 2a). The distributions of stress ratio and the horizontal principal deviatoric stress axes demonstrate that normal faulting and strike-slip faulting regimes are broadly dominant in the southern half of the Pacific plate. In particular, in the French Polynesia region, where some hotspots with large buoyancy fluxes have been observed, the compressional stress is generally dominant in the east-west direction.

In contrast, the northern part of the Pacific plate is dominated by a thrust faulting regime in which the direction of tensional stress axes in the stable and older parts of the Pacific plate tend to be oblique along the direction of plate motion. This result implies that the stress state is nearly neutral (i.e., neither compressional nor tensional) along the direction of the plate motion. On the other hand, the compressive horizontal principal deviatoric stress axes are nearly perpendicular to the Japan and Izu-Ogasawara Trenches, which is consistent with the observation data [1].

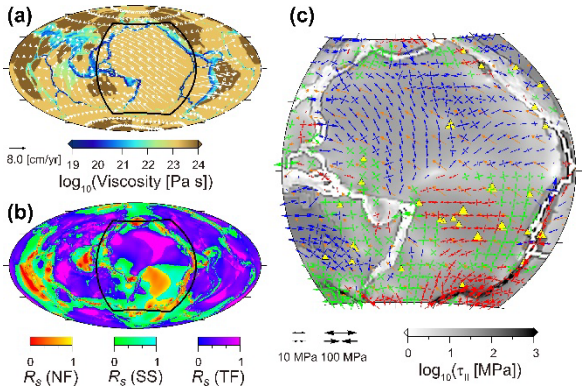

Fig. 2. Numerical results for "Model Ref" [2] with a viscosity contrast between the lithosphere and the upper mantle of 300 and a viscosity contrast between the lower and upper mantle of 30. (a) Viscosity and horizontal velocity fields near the entire top surface boundary. (b) Stress ratio, R_s, in each faulting regime near the entire top surface boundary. "NF", "SS", and "TF" indicate the normal, strike-slip, and thurst faulting regimes. (c) Horizontal principal deviatoric stress axes in the Pacific plate enclosed by solid lines in (a) and (b). The red, green, and blue axes indicate the NF, SS, and TF regimes. Modified from Fig. 5 of [2].

Therefore, there is a dichotomy of stress regimes between the two hemispheres: the thrust faulting regime is dominant in the northern Pacific, whereas the normal faulting regime is dominant in the southern Pacific. The present numerical studies suggest that the entire Pacific plate inherently maintains a neutral stress-state in both the northern and southern parts of the Pacific Plate, but the stress regime of the southern part is affected by large-scale upwelling flow originating from the Large Low-Velocity Provinces (LLVPs) under the South Pacific.

Figure 2c demonstrates that the square root of the second invariant of deviatoric stress (τ_{II}) is generally in the order of 10 MPa and not larger than 100 MPa in the stable part of the Pacific plate, whereas the viscosity of weak plate boundaries is lower than the order of 1 MPa. These stress magnitudes are comparable to those in the stable part of the plates and plate boundaries of the Earth and are not significantly different from those even for the other models studied in this study.

4. Concluding Remarks

The present numerical studies demonstrated the southern part of the Pacific plate is dominated by a normal faulting regime, whereas the northern part is dominated by a thrust faulting regime. The tensional stress axes in the older and stable part of the Pacific plate tend to be oblique to the direction of plate motion, which suggests that the stress state of the Pacific plate is almost neutral along the direction of plate motion. It is recognized that the intraplate stress on a global scale reflects the force acting on the base of the plate through a mechanical coupling between plate motion and the underlying asthenospheric flow [e.g., 6]. In the future, I will investigate the relationship between intraplate stress and the driving force of the Earth's major oceanic plate using a numerical model with improved spatial resolutions.

Acknowledgement

Numerical calculations in the present study were mainly performed on the supercomputer facilities of the DA system and partly performed on the Earth Simulator (ES4) at JAMSTEC.

References

[1] O. Heidbach, et al. "The World Stress Map database release 2016: Crustal stress pattern across scales," *Tectonophys.* vol. 744, pp. 484–498, 2018.

[2] M. Yoshida. "Stress state of the stable part of the Pacific plate predicted by a numerical model of global mantle flow coupled with plate motion," *Lithosphere*. vol. 2023, no. 1, pp. 6563534, 2023.

[3] C. Lu, S.P. Grand, H. Lai, and E.J. Garnero. "TX2019slab: A New P and S tomography model incorporating subducting slabs," *J. Geophys. Res. Solid Earth.* vol. 124, no. 11, pp. 11549–11567, 2019.

[4] G.P. Hayes, et al. "Slab2, a comprehensive subduction zone geometry model," *Science*. vol. 362, no. 6410, pp. 58–61, 2018.

[5] M. Yoshida. "A new analysis of the intraplate stress regime and stress ratio in numerically modeled mantle convection," *Tectonophys*. vol. 826, pp. 229240, 2022.

[6] M. Yoshida. "How mantle convection drives the supercontinent cycle: Mechanism, driving force, and substantivity," In: João C. Duarte (Ed.), *Dynamics of Plate Tectonics and Mantle Convection*. pp. 197–221, Elsevier, Amsterdam, Netherlands, 2023.